CHEMICAL ENGINEERING TRANSACTIONS
VOL. 51, 2016
A publication of AIDIC
The Italian Association of Chemical Engineering
Online at www.aidic.it/cet
Guest Editors: Tichun Wang, Hongyang Zhang, Lei Tian

ISBN 978-88-95608-43-3; **ISSN** 2283-9216
DOI: 10.3303/CET1651013

Numerical Simulation of Abrasive Water Jet Cutting Chemical Pipeline Based on SPH Coupled FEM

Lianhuan Guo[a], Songsheng Deng[a], Xin Yang*[b]

[a]Department of Military Oil Supply Engineering, Logistic Engineering University of PLA, Chongqing 401331, China
[b]Department of Industrial & Manufacturing Engineering, Florida State University, Tallahassee 32304, United States
xyang2@fsu.edu

Abrasive water jet (AWJ) is an advanced machining technology, which presents better cutting quality than traditional machining methods. Because the large deformation in finite element method (FEM) tends to produce mesh distortion, this paper enables simulation of AWJ cutting steel by adopting smoothed particle hydrodynamics (SPH) coupled FEM. Abrasive and water are modeled by SPH particles, target is modeled by FE. The distribution of two kinds of SPH particles is realized through modifying the keyword file and the impact velocity of SPH particles is obtained through computational fluid dynamics (CFD). Simulation results clearly show the change to kerf sectional shape. The relation curves between cutting depth and AWJ parameters, including pressure and transverse speed, are consistent with the experimental results, which proves the effectiveness of simulation method.

1. Introduction

Compared with traditional machining methods, AWJ cutting technology is characterized by its cold state and high safety. It produces no heat stress, flame or poisonous and harmful gas in operation, which makes AWJ applicable to metal and non-metallic material cutting and widely used in chemical, petroleum and mining industries (Hashish, 1984). Depending on the way of mixing between abrasive and water, AWJ can be pre-mixed or post-mixed. This paper focuses on the pre-mixed AWJ cutting technology.

AWJ cutting process involves many parameters. At present, experimental method is mostly relied on for the study of influence of each parameter on the cutting performance (Hassan et al., 2004). Momber and Kovacevic (1988) reorganized the experimental data of AWJ and analyzed the law of influence of various parameters on the cutting depth. Limited by the experimental conditions, the experiment generally costs high, and some scholars began to use numerical simulation for research. Ma et al. (2008) used FEM, ALE and SPH to simulate pure water cutting low-carbon steel and found that FEM had mesh distortion which caused computation termination, ALE usually required large computation, yet SPH achieved efficient simulation analysis. Yu et al. (2012) simulated the acceleration process of abrasive particles in the post-mixed nozzle and, in the modeling, water used SPH particles and abrasive used FEM element. Lin et al. (2014) used SPH coupled FEM to simulate the damage field and range of rock crushing pit under the influence of AWJ.

Due to air entrainment, the jet velocity will attenuate with the increase of target distance. Moreover, due to the large inertia of abrasive particles, velocity difference will be generated between abrasive particles and water. However, few literature have considered such influence on simulation. As an important parameter in the simulation, the accuracy of jet velocity assignment directly affects the simulation results, in order for more practical velocity assignment, CFD is used to solve the impact velocity of abrasive particles and water under non-submerged conditions. After the velocity is assigned to SPH particles, method of SPH coupled FEM is used to simulate the erosion process of steel.

2. Simulation

The simulation consists of two parts: a. obtaining of the impact velocities v_a of abrasive particles and v_w of water by CFD; b. to simulate the impact process of particles on the target by SPH coupled FEM. The velocity obtained from the former will be assigned to SPH particles of the latter.

Please cite this article as: Guo L.H., Deng S.S., Yang X., 2016, Numerical simulation of abrasive water jet cutting chemical pipeline based on sph coupled fem, Chemical Engineering Transactions, 51, 73-78 DOI:10.3303/CET1651013

2.1 Computation of impact velocity

Software Fluent is used to calculate the impact velocity, which is CFD business software based on finite volume method and has been widely used in AWJ flow field simulation (Huang et al., 2007; Dimitrios et al., 2015). As shown in Figure 1, a 3D model including nozzle and air domain is built, in which the nozzle is comprised of conical contraction section and cylindrical section, and the air domain serves as the exterior region of the nozzle. Pressure inlet boundary conditions are taken for the inlet. Pressure outlet boundary conditions are taken for the outlet by referring to an exclusive standard atmospheric pressure.

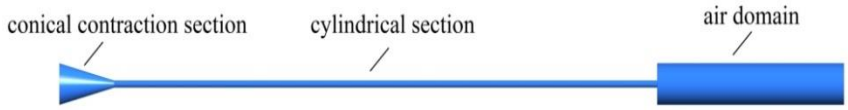

Figure 1: Nozzle and air domain model

Velocity contour in the air domain under 40 MPa is shown in Figure 2. Velocity contour under other pressure can be obtained in the same way, including 25 MPa, 30 MPa, 35 MPa, and 45 MPa.

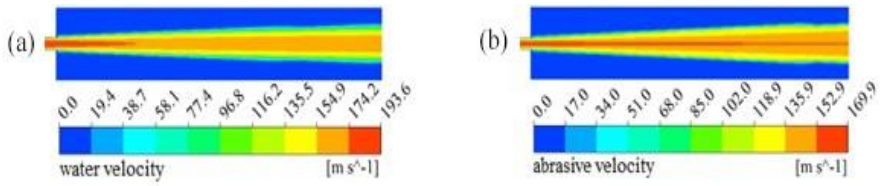

Figure 2: Velocity contour in air domain under 40 MPa: (a) water velocity v_w, (b) abrasive velocity v_a.

Figure 3(a)-(b) show the axial velocity attenuation curve of abrasive particles and water outside the nozzle. It can be seen that there is certain velocity difference between water and abrasive particles and the attenuation of abrasive particle velocity is slower than that of water, because the density of abrasive particles is greater than water, causing larger inertia. The impact velocities v_w and v_a can be extracted from the velocity curves under different pressure. The change in transverse speed doesn't affect the impact velocity of particles, v_w and v_a are 177.9 m/s and 161.1 m/s respectively. In the keyword file of LS-DYNA, V_x and V_y are defined as transverse speed and impact velocity respectively.

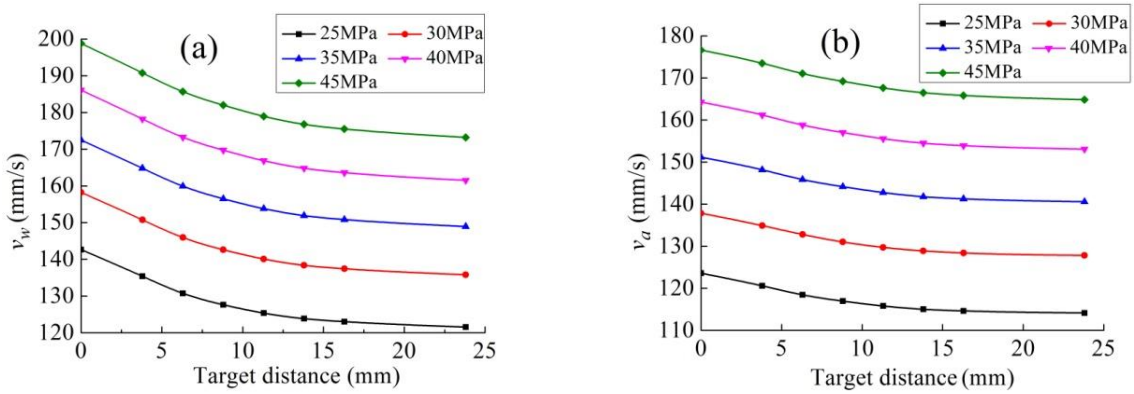

Figure 3: Axial velocity attenuation curve: (a) water axial velocity v_w, (b) abrasive axial velocity v_a.

2.2 Simulation of SPH coupled FEM

1. SPH fundamentals

SPH requires no mesh and represents fluid with a series of particles, which have all properties of the fluid (Liu et al., 2003). In SPH, the integral expression of the field variable f(x) can be expressed as:

$$f(x)=\int_{\Omega} f(y)\delta(x-y)\mathrm{d}y \tag{1}$$

Where Ω is the integration domain of x. Function $\delta(x-y)$ is approximately replaced with kernel function $W(x-y, h)$, and $f(x)$ can be expressed as:

$$f(x)=\int_{\Omega} f(y)W(x-y,h)\mathrm{d}y \tag{2}$$

Where h is smoothing length, which changes over time: Particle approximation method is used to approximately place the voxel dy at particle j with particle volume ΔV_j, and $f(x)$ can be written in discrete form:

$$f(x)\approx\sum_{j=1}^{N}\frac{m_j}{\rho_j}f(x_j)W(x-x_j,h_i) \tag{3}$$

Its gradient function is:

$$\nabla f(x_i)=\sum_{j=1}^{N}\frac{m_j}{\rho_j}f(x_j)\nabla_i W(x_i-x_j,h_i) \tag{4}$$

Formula (4) is applied to the density field ρ_i, in consideration of the continuity equation of fluid mechanics, the control equation is as follows:

$$\frac{\mathrm{d}\rho_i}{\mathrm{d}t}=\sum_{j=1}^{N}m_j(v_i-v_j)\nabla_i W(x_i-x_j,h_i) \tag{5}$$

The momentum and energy equation in differential form can be obtained:

$$\frac{\mathrm{d}v_i}{\mathrm{d}t}=\sum_{j=1}^{N}m_j\left(\frac{p_i}{\rho_i^2}+\frac{p_j}{\rho_j^2}+\prod_{ij}\right)\nabla_i W(x_i-x_j,h_i) \tag{6}$$

$$\frac{\mathrm{d}e_i}{\mathrm{d}t}=\frac{1}{2}\sum_{j=1}^{N}m_j\left(\frac{p_i}{\rho_i^2}+\frac{p_j}{\rho_j^2}+\prod_{ij}\right)v_{ij}\nabla_i W(x_i-x_j,h_i) \tag{7}$$

Where $v_{ij}=(v_i-v_j)$, Π_{ij} is artificial viscosity.

2. Definition of material model

The material constitutive model is the basis for numerical simulation, and the modeling in this article contains abrasive, water and target. *MAT_Null material model is selected for water, whose pressure is calculated by the state equation Mie-Grueisen in Formula (8). Constant coefficient setting in Formula (8) can be obtained from reference (Lin et al., 2014).

$$P=\frac{\rho_O C^2\mu\left[1+\left(1-\frac{\gamma_O}{2}\right)\mu-\frac{a}{2}\mu^2\right]}{\left[1-(S_1-1)\mu-S_2\frac{\mu_2}{\mu+1}-S_3\frac{\mu^3}{(\mu+1)^2}\right]}+(\gamma_O+a\mu)Ea \tag{8}$$

Taking brown fused alumina as the abrasive particles, *MAT_ELASTIC model is adopted. Material parameters are provided in Table 1. The plastic hardening material model is selected for the target and the failure strain ε is set so that the erosion of material can be confirmed depending on whether the strain values exceeds the failure strain; if so, the element is determined as failure and deleted. If all associated elements around a node fail, the node is removed. X60 steel is taken as target material and keyword *MAT_PLASTIC_KINEMATIC is used to define the material properties of target. See Table 2 for the parameters of target.

SPH particles are used for both abrasive and water, but the two kinds of particles have their own material properties. In this paper, the spatial distribution of two kinds of SPH particles is achieved by means of Matlab software programming and the programmed content is imported into keyword file of LS-DYNA. Figure 4 shows a schematic view of the spatial distribution of SPH particles, in which the blue represents SPH particle element of water and the brown represents SPH particle element of abrasive.

Table 1: Parameters of abrasive particle

Parameter	Value
Density, ρ_a (kg/m^3)	3970
Elasticity module, E (GPa)	450
Poisson's coefficient, μ	0.25

Table 2: Parameters of target

Parameter	Value
Density, ρ_m (kg/m^3)	7900
Elasticity module, E (GPa)	204
Poisson's coefficient, μ	0.3
Yield stress, σ_s (MPa)	416
Tensile strength, σ_b (MPa)	512
Failed strain, ε	0.18

3. Boundary conditions

The target is 50 mm long, 10 mm wide and 40 mm high, and the mesh is generated with 8-node hexahedral element. As required by the simulation, AWJ is set as a 60 mm-high cylinder with a diameter of 0.8 mm, and there are a total of 4,995 SPH particle elements in the model. To eliminate the reflection of stress wave, NON_REFLECTING boundary conditions are applied. Degree of freedom in every direction of bottom surface is bound so as to avoid rigid motion. SPH coupled FEM will be achieved through contact algorithm CONTACT_ERODING_NODES_TO_SURFACE. Figure 5 shows the coupling process, where the left and right sides are respectively computation processes of SPH and FEM (Attaway et al., 1994).

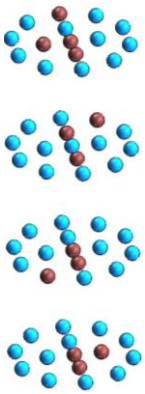

Figure 4: Spatial distribution of SPH particles

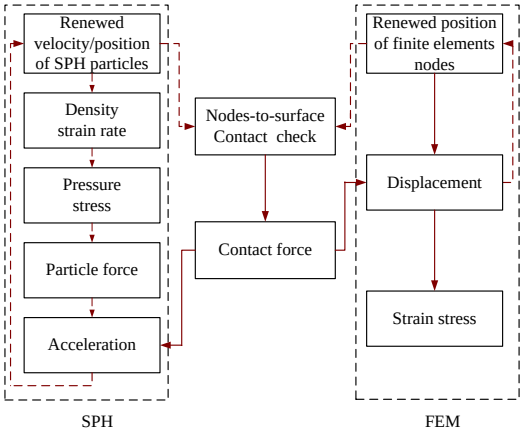

Figure 5: Coupling process of SPH and FEM

3. Simulation results and analysis

Figure 6 shows the sectional shape changes of kerf under 30 MPa. In the initial phase, the metal surface is affected by the ductile shear effect of jet, and the metal element in central region of jet effect is damaged. When the strain value exceeds failure strain, the element will be removed, and the target section produces a shallow V-shape kerf, as shown in Figure 6(a); as the erosion go on, some jet particles continue to play a part in increasing the cutting depth, other particles erode the kerf wall to widen it, and the section shows a deep V-shape kerf, as shown in Figure 6(b); finally, since the cutting depth stabilizes and the target body isn't cut through, the rebounding particles still have some energy and continue to erode the bottom area of kerf, and the bottom changes into the U shape gradually from V shape, as shown in Figure 6(c)-(d).

The simulation results clearly reflects the change in the cutting depth, which increases rapidly within 0-170 μs and reaches 4.8 mm at 170 μs. Then, the cutting depth grows slowly, which reaches 6.9 mm at 350 μs and eventually stabilizes around 7 mm. It can be seen from the increase trend of cutting depth, there is no a linear increase relationship between the changed cutting depth and the computation time, and when the computation time reaches a certain value, the cutting depth becomes stable. This is attributable to jet erosion of the target completed in a very short time. As the cutting depth increased, a water cushion forms at the bottom of kerf and acts as a buffer which weakens the jet erosion. In addition, for the cutting perpendicular to the workpiece surface, abrasive and water rebound obviously, and the strike between rebounded particles and flow particles also exhausts the kinetic energy of subsequent jet particles. Figure 11 has reflected the rebound and scattering of particles very well.

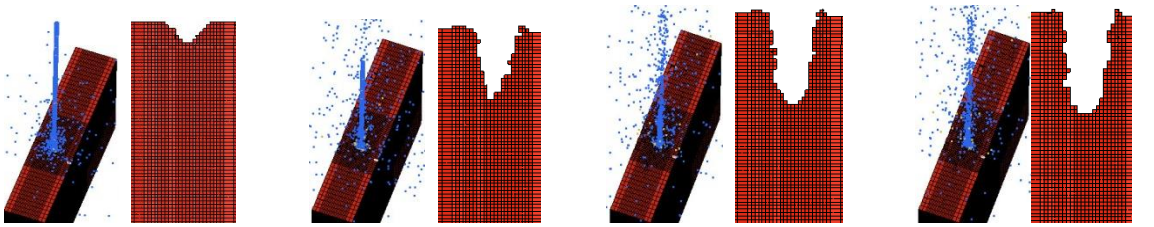

(a) t=50 *μs* (b) t=170 *μs* (c) t=305 *μs* (d) t=350 *μs*

Figure 6: Sectional shape changes *of kerf*

3.1 Relationship between cutting depth and pressure

According to Table 3, simulation results h_s is found with an error of 1.6-7.4 % against experimental results h_e at various pressure.

Table 3: Error analysis

p (MPa)	h_s (mm)	h_e (mm)	Error (%)
25	5.73	5.64	1.6
30	7.06	6.65	6.2
35	8.81	8.20	7.4
40	10.64	10.27	3.6
45	12.63	12.06	4.7

Table 4: Error analysis

u (mm/min)	h_s (mm)	h_e (mm)	Error (%)
30	16.31	15.32	6.5
40	13.12	12.54	4.6
50	10.64	10.27	3.6
60	8.02	7.15	12.2
70	5.95	5.23	13.8

3.2 Relationship between cutting depth and transverse velocity

According to Table 4, the error range between simulation results h_s and experimental results h_e is 3.6-13.8 % at various transverse velocity.

As can be seen from the curves in Figure 7, when the pressure increases, the cutting depth grows. There is an approximately linear increase relationship between cutting depth and pressure. With the increase of pressure, impact velocity of particles is improved and particles can get greater kinetic energy, so the cutting capability of jet is enhanced. Regression curve between cutting depth and pressure is obtained after curve fitting, and the regression function is expressed as: h=0.352p-3.34. The function expression shows that there is a threshold pressure of 9.5 MPa in such condition, and when pressure drops to the threshold, cutting depth is close to zero, AWJ can't cut target any more.

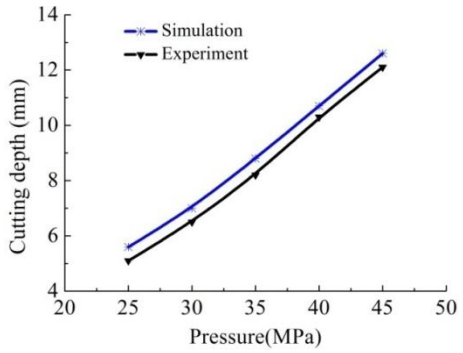

Figure 7: Curves of cutting depth and pressure

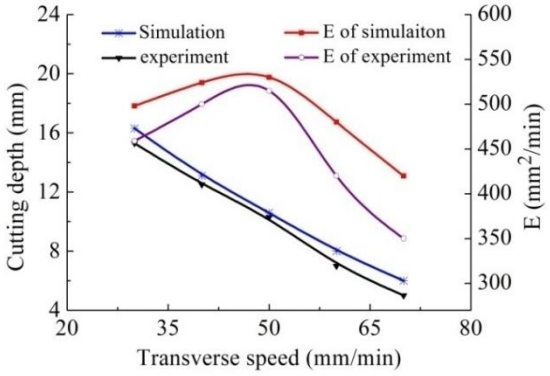

Figure 8: Curves of cutting depth and transverse speed

As shown in Figure 8, when the transverse speed increases, the cutting depth decreases, which shows a similar exponential decrease law. This is because with the increasing transverse speed, the number of particles impacting the same section reduces, leading to a lower material removal rate. After curve fitting, the regression curve between cutting depth and transverse speed is obtained, and the regression function can be expressed as $h=35.65e^{-0.02u}$. Although the lower transverse speed makes cutting depth increase, it does not mean improved cutting efficiency E which is the product of cutting depth and transverse speed. Further analysis of cutting efficiency E at different speed shows that E value increases first and then decreases,

therefore to enhance cutting efficiency, the transverse speed is required within a certain reasonable limit. Figure 14 shows that when the transverse speed is about 50 mm/min, cutting efficiency E will reach the maximum.

4. Conclusions

In this paper, meshless SPH modeling for water and abrasive avoids mesh distortion in the simulation process. Moreover, FEM modeling for target can take advantage of its high computation accuracy, making it easy to track changes to kerf sectional shape and cutting depth. In this paper, SPH coupled FEM method is used to effectively simulate AWJ cutting steel. The simulated changes in kerf sectional shape help visualize the kerf formation process and material erosion process, which can't be obtained through experimental means. Meanwhile, the simulated p-h and u-h curves are consistent with the experimental results, and the error is within a reasonable range. However, due to more process parameters in AWJ cutting, further simulation analysis can be carried out for other parameters such as abrasive concentration and jet angle, etc., to improve the numerical simulation of AWJ.

Acknowledgments

The research team acknowledges the financial support by the project from General Logistics Department of PLA (No.YX213C208).

References

Attaway S. W., Heinstein M. W., Swegle J. W., 1994, Coupling of smooth particle hydrodynamics with the finite element method, Nuclear Engineering and Design, 150, 199–205, DOI : 10.1016/0029-5493(94)90136-8.

Dimitrios P., Simon L., 2015, Advance in CFD modelling of multiphase flows in cyclone separators, Chemical Engineering Transactions, 43, 1603-1608, DOI: 10.3303/CET1543268.

Hashish M., 1984, A model study of metal cutting with abrasive water jets, ASME Journal of Engineering Materials and Technology, 106, 88-100, DOI: 10.1115/1.3225682.

Hassan A. I., Chen C., Kovacevic R., 2004, On-line monitoring of depth of cut in AWJ cutting, International Journal of Machine Tools and Manufacture, 44, 595–605, DOI: 10.1016/j.ijmachtools.2003.12.002.

Huang C. Z., Hou R. G., Wang J., Lu X. Y., Zhu H. T., 2007, Three-dimensional simulaiton of liquid-solid two-phase flow inside the abrasive water jet nozzle, Key Engineering Materials, 329, 329-334, DOI: 10.4028/www.scientific.net/KEM.329.329.

Lin X. D., Lu Y. Y., Tang J. R., Ao X., Zhang L., 2014, Numerical simulation of abrasive water jet breaking rock with SPH-FEM coupling algorithm, Journal of Vibration and Shock, 33, 170-176, DOI: 10.13465/j.cnki.jvs.2014.18.028.

Liu G. R., Liu M. B., 2003, Smoothed Particle Hydrodynamics: A Mesh-Free Particle Method, World Scientific Publishing Co Ltd, Singapore.

Ma L., Bao R. H., Guo Y. M., 2008, Waterjet penetration simulation by hybrid code of SPH and FEA, Iniemational Journal of Impact Engineering, 35, 1035-1042, DOI: 10.1016/j.ijimpeng.2007.05.007.

Momber A. W., Kovacevic R., 1988, Principles of Abrasive Water Jet Machining, Springer, London.

Pierre L., Frédéric H., Laurent A., Anne J., Pierre S., 2015, 2D modeling of turbulent flow around a cylindrical storage tank by artificial neural networks, Chemical Engineering Transactions, 43, 1621-1626, DOI: 10.3303/CET1543271.

Yu F., Wang J. M., Liu F. H., 2012, Numerical simulation of single particle acceleration process by SPH coupled FEM for abrasive waterjet cutting, International Journal of Advanced Manufacturing Technology, 59, 193-200, DOI: 10.1007/s00170-011-3495-z.